九州大学学術情報リポジトリ
Kyushu University Institutional Repository

THE HIGH FREQUENCY SPECTRUM OF WINDGENERATED WAVES

MITSUYASU, Hisashi
Research Institute for Applied Mechanics, Kyushu University: Professor

HONDA, Tadao
Research Institute for Applied Mechanics, Kyushu University: Research Associate

https://doi.org/10.5109/7173512

出版情報：Reports of Research Institute for Applied Mechanics. 22 (71), pp.327-355, 1975. 九州大学応用力学研究所
バージョン：
権利関係：

KYUSHU UNIVERSITY

Reports of Research Institute for Applied Mechanics
Vol. XXII, No. 71, 1975

THE HIGH FREQUENCY SPECTRUM OF WIND-GENERATED WAVES*

Hisashi MITSUYASU** and Tadao HONDA***

The high frequency part (10 Hz～50 Hz) of the one-dimensional wave spectrum was measured in a wind-wave channel under accurately controlled conditions. The results are compared with the spectral forms for the capillary range that have been proposed recently by PIERSON and STACY (1973) and TOBA (1973). In a general sense, fairly good agreement is found between the present results and those of PIERSON and STACY (1973) and of TOBA (1973). The spectrum in the capillary range is clearly wind speed dependent, and the spectral density in that range increases with increasing wind speed.

However, closer examination shows systematic deviations of the present results from those previously proposed, particularly for high speed winds.

1. Introduction

The energy of ocean waves is distributed continuously with regard to various frequencies and also various directions. Therefore, ocean waves can be described by the two dimensional wave spectrum. Although a great many studies have been done on the one-dimensional frequency spectrum of the ocean waves, many of them were concerned with the dominant part of the wave spectrum which is in the gravity wave range (NEUMANN[1], PIERSON and MOSKOWITZ[2], BRETSCHNEIDER[3], MITSUYASU[4]). This is due to the fact that most of the wave energy concentrates in the dominant part of the spectrum with a relatively narrow frequency range where the gravitational acceleration, g, is a main controlling factor.

However, the high frequency part of the ocean wave spectrum, which is almost in the gravity-capillary range and the capillary range, is also important for various problems, though the spectral energy in these range is relatively small. For examples, the high frequency wave spectrum has an important role in the following problems; 1) water surface roughness (MUNK[5]), 2) momentum transfer from the wind to the wave (LONGUET-HIGGINS[6]), 3) nonlinear interactions among gravity-capillary waves (MC-GOLDRICK[7], VALENZUELA and LAING[8]), 4) backscatter of electro-magnetic waves from the sea surface (PIERSON, et al[9], PIERSON and

*This paper was originally presented in Journal of the Oceanographical Society of Japan Vol. 30, 1974. Some data are added at this time.

**Professor, Research Institute for Applied Mechanics, Kyushu University.
***Research Associate, Research Institute for Applied Mechanics, Kyushu University.

STACY [10]).

In spite of the increasing need for accurate information on high frequency wave spectra, reliable data are very few except for the slope spectra of laboratory wind waves measured by COX [11] and several pioneering studies (PIERSON and STACY [10], TOBA [12]). In a recent paper, PIERSON and STACY proposed a spectral form for very wide frequency ranges using a wide variet of reports and data sources. They also showed that the capillary range of the wave spectrum is strongly wind speed dependent and that there is no equilibrium capillary range, at least for winds up to 30 m/s. Independently, TOBA also proposed a high frequency wave spectrum which gives frequency and wind speed dependentes as $u_* f^{-4}$, where f is the frequency of the spectral component and u_* is the friction velocity of the wind. Although the results of these studies were very important for shedding light on the high frequency wave spectrum, their data of the wind-generated waves were unfortunately not necessarily best for a study of high frequency part of the wave spectrum. That is, the frequency response of the wave recording systems was not clearly checked, and the frequency ranges of the measured wave spectra did not cover sufficiently high frequencies.

The present study is designed mainly to clarify the high frequency part of the one-dimensional spectrum of wind-generated waves, where the effect of the surface tension becomes increasingly dominant. Therefore, the frequency response of the wave recording system was carefully checked first, and one-dimensional frequency spectra of wind waves generated in a laboratory tank were measured under various controlled conditions

2. Equipment and techniques

2.1 Wind-wave channel

Wind waves were generated in a wind-wave channel, schematically shown in fig. 1. The channel consists of a wind blower section, a glass-enclosed test section and an exhaust section. The inside dimensions of the test section are 60 cm wide, 80 cm high and 8.51 m long At the wind-blower side of the channel a transition plate with artificial roughness was inserted to thicken the boundary layer of the air flow above the water surface The

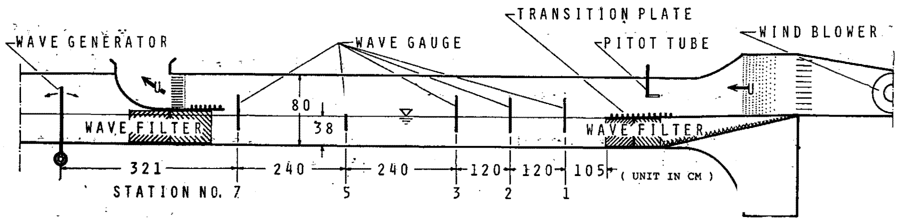

Fig. 1 General scheme of the wind-wave facility.

wave generator and the transition plate at the exhaust section have no relation to the present experiment. Five wave gauges were installed at measuring stations No. 1, No. 2, No. 3, No. 5, and No. 7. The corresponding fetch of each station is as follows:

Station No.	1	2	3	5	7
Fetch F (cm)	105	225	345	585	825

A standard Pitot-static tube was set 20 cm above the transition plate at the wind-blower side to monitor the reference wind speed in the channel. The wind speed measured by this Pitot-static tube will be refered as the reference wind speed Ur, which corresponds approximately to the mean wind speed in the test section. The following five wind speeds were used in the experiment:

Ur: 5, 7.5, 10, 12.5, 15 m/s

The water depth was set to be 38 cm before the start of the measurement. Wind-generated waves propogated in the test section growing gradually and were absorbed by wave filters at the exhaust section.

2.2 Wave measuring techniques

Wind-generated waves were measured by resistance-type wave gauges of two different kinds. One was a single platinum wire with a diameter 0.1 mm, and the other was two parallel platinum wires with the same diameter and 2 mm separation. Because the linear range of the calibration curve was not as wide for the wave gauges of the single-wire type, they were used at stations No. 1, No. 2, and No. 3, where the wave heights were relatively small. The wave gauges of the parallel-wire type had a sufficienty

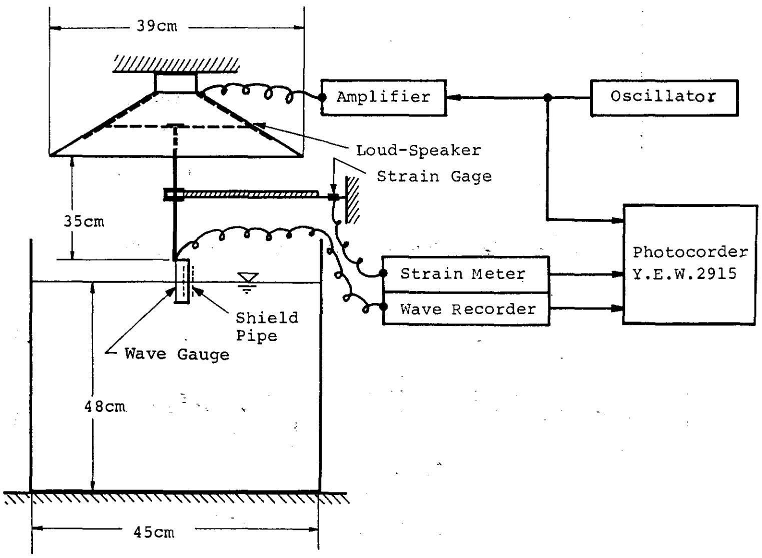

Fig. 2 Schematic diagram for the measurements of response of wave gauges.

wide range for linear calibration curve, and they were used at the stations No. 5, and No. 7. As electronic circuits for the wave gauges, a 6 channel dynamic strain meter of a standard type, which consists of bridge circuits, an oscillator (5 KHz), carrier amplifiers and discriminator, was used.

Since the high frequency part of wind-generated waves was being studied, the frequency response of the wave gauge must be uniform up to sufficiently high frequencies. The frequency response of the wave gauge was tested by using the calibration setup shown schematically in Fig. 2.

Fig. 3 shows the frequency response of the wave gauges. It can be seen from the results shown in Fig. 3. that the amplitude response factor is approximately unity up to 40 Hz for the parallel-wire wave gauge and up to 80 Hz for the single-wire wave gauge. The small peak of the response of the parallel wire at near 30 Hz is considered, from the time history of the recorded signal, to be due to the oscillation of a mass of water that climbed up between the probe wires because of surface tension effects.

As a prewhitening technique for the measurement of the high frequency

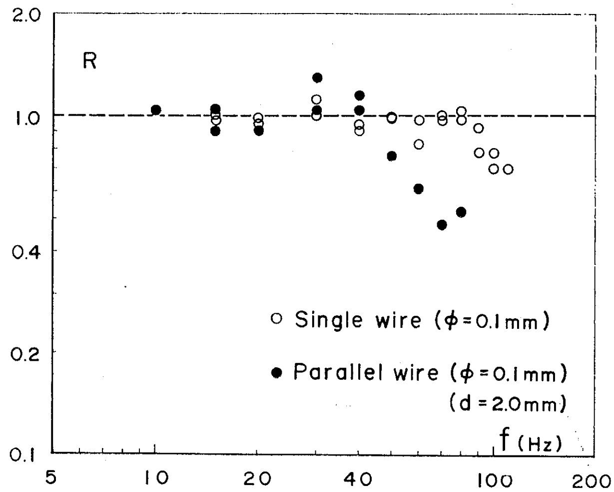

Fig. 3 Amplitude response factors of the wave gauges.

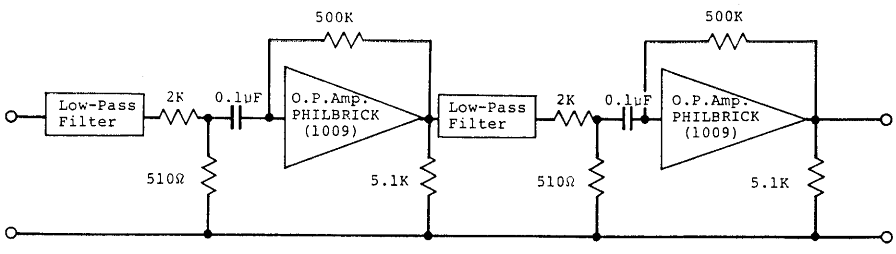

Fig. 4 Differentiation circuit.

wave spectrum, the electronic differentiation circuit shown in Fig. 4 was used. The differentiation circuit is also convenient for visualizing the tiny ripples superimposed on the dominant wind waves, because as will be shown later in Fig. 10, it amplifies greatly the high frequency components of the wind waves. Low-pass filters with cut-off frequency 56 Hz were used to eliminate the noise related to the power source at 60 Hz.

Examples of the frequency response of the differentiation circuit combined with low-pass filters are shown in Fig. 5.

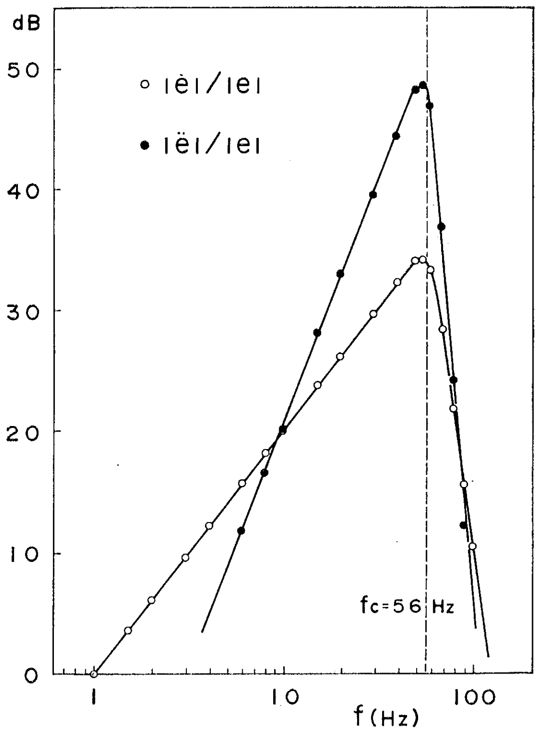

Fig. 5 Calibration of the differentiation circuit.

In a frequency range below the cut-off frequecy the differentiations are shown to be almost complete.

2.3 Experimental procedures

Fig. 6 shows the general scheme for the measuring system. Waves were measured simultaneously at the five stations. The outputs of the wave gauges at the stations No. 1, No. 2 and No. 3 were sent respectively to the differentiation circuits to obtain the vertical velocity, $\dot{\eta}(t)$, and vertical acceleration, $\ddot{\eta}(t)$, which were recorded simultaneously with the surface

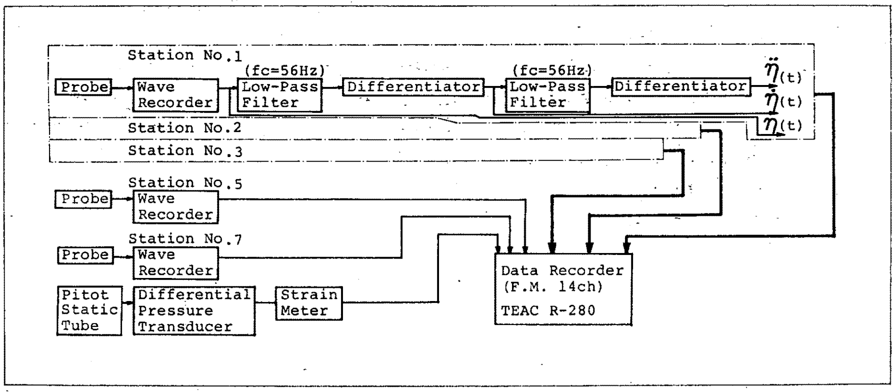

Fig. 6 General scheme of measuring system.

elevation, $\eta(t)$. In order to monitor the wind speed during the wave measurement, the Pitot-static tube shown in Fig. 1 was connected to the dynamic strain meter through a differential-pressure transducer, and an electronic signal which was proportional to the dynamic pressure $\rho U_r^2/2$ was recorded. All signals were recorded simultaneously on a 14-channel data recorder and were monitored by means of two chart recorders; one is 8-channel and the other is 6-channel.

The wind speed was changed stepwise from 0 to Ur=15 m/s as shown in Fig. 7, and the wind-generated waves were measured continuously during this course. Therefore, the wave record included both the transition parts that occurred a little after the time when the wind speed changed to the next speed and the statistically stationary parts that were caused when the

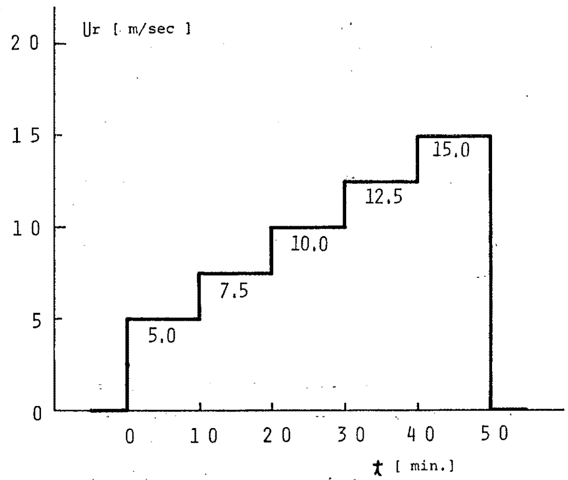

Fig. 7 Time history of the wind speed in the wind-wave channel

wind of constant speed continued to blow. The wave gauges were carefully calibrated before and after the wave measurement.

Experimental conditions monitored before and after the measurements are as follows;

Air temperature T_a; 14.0～13.0°C
Water temperature T_w; 11.0°C
Atmospheric pressure P_a; 765.7～764.0 mmHg
Water depth d; 38.5～37.8 cm*)

2.4 Spectal analysis of the wave data

The wave data recorded on the magnetic tape were reproduced and digitized by using a high speed A-to-D converter (DATAC-500). The spectral analysis of the data was done on a FACOM 270-20 computer using a standard program based on fast Fouier transform procedures.

In the analysis, only the wave data corresponding to the statistically stationary parts were used. A stationary part of the wave record, 102.4 sec long, was picked from 10 minut long wave record corresponding to each wind speed, and it was divided into segments (samples). The spectral analysis was done using the wave data from each segment of 10.24 sec long (data points 2048). Fig. 8a shows an example of raw spectra. Then, mean

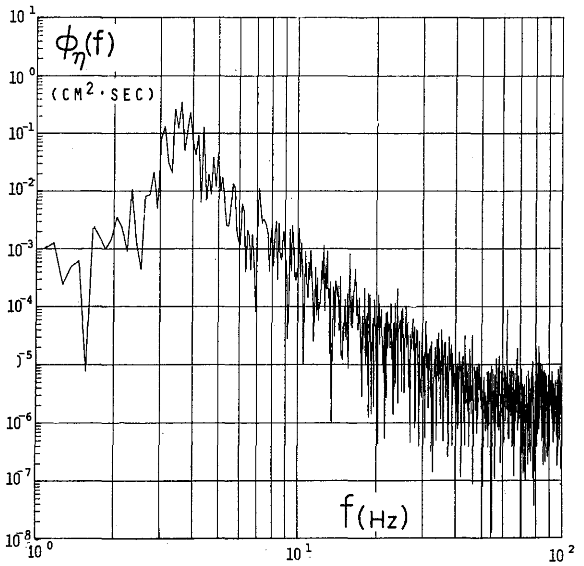

Fig. 8a Raw spectrum of one sample of wave data.
(F=585 cm, U_r=12.5 m/s)

*Slight decrease of the water depth was found after the experiment. This is due to the fact that a small amount of water was blown out of the tank by the high speed wind.

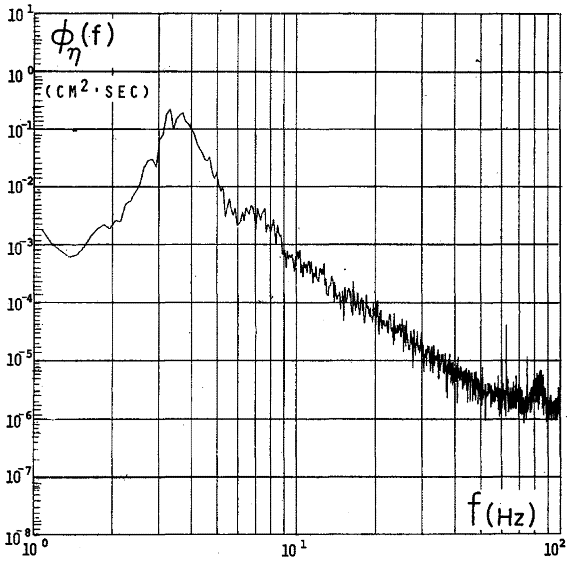

Fig. 8b Mean of raw spectra of ten samples of wave data.

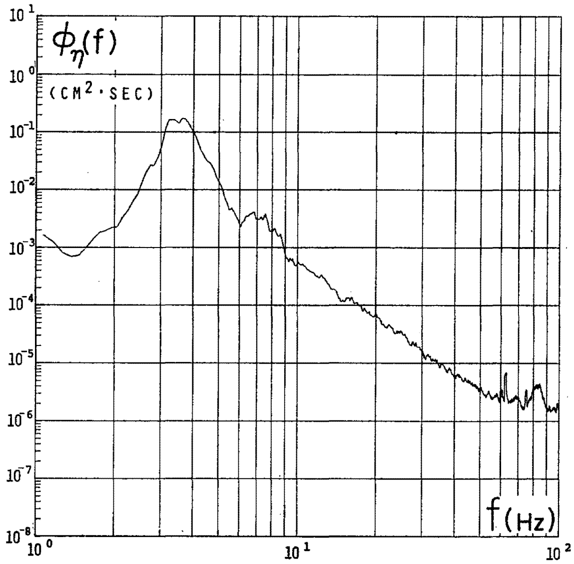

Fig. 8c Filtered spectrum

was taken by using ten sample of the raw wave spectra corresponding to each experimental condition. An example of the mean spectrum is shown in Fig. 8b. Finally, the following average was computed for the mean spectrum;

three line moving average; $f=0\sim10$ Hz,
eleven line moving average; $f=10\sim100$ Hz.

In the high frequency region of the spectrum, the change of the spectral density is relatively smooth except for irregular zigzag form due to the statistical errors. Therefore, the width of the spectral filter (the number of the spectral lines for moving average) was increased as compared with that used for the low frequency range. An example of the spectra finally obtained is shown in Fig. 8c.

The conditions relating to the data analysis are summarized as follows:

Sampling frequency; 200 Hz
Nyquist frequency; 100 Hz
Data length (per one sampl); 10.24 sec
Data point (per one sample); 2048
Number of sample; 10 samples
Spectral analysis; FFT method
Spectral filter; moving average of successive three line spectra for the frequency range $f=0\sim10$ Hz, moving average of successive eleven line spectra for the frequency range $f=10$ Hz~100 Hz.
Equivalent degrees of freedom; $k \doteqdot 60$ for $f=0\sim10$ Hz, $k \doteqdot 220$ for $f=10\sim100$ Hz.

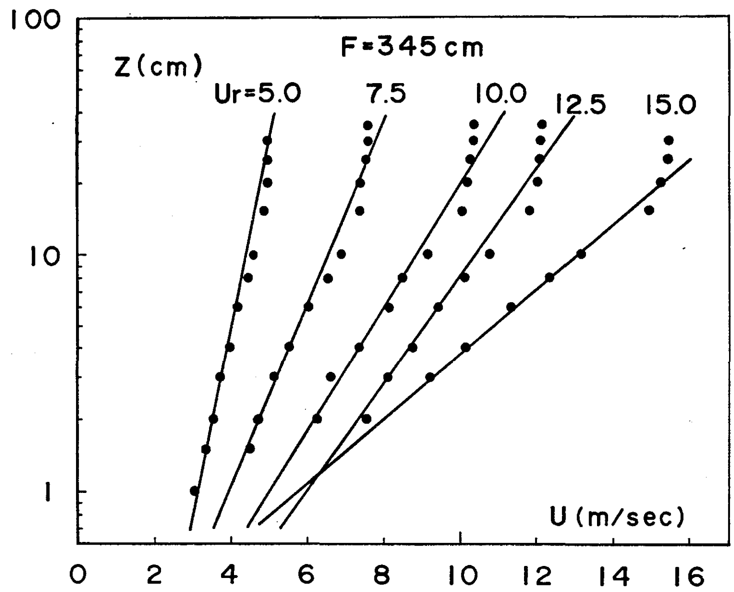

Fig. 9 Wind profiles over the water surface. (F=345 cm)

3. Results of the preliminary analysis

3.1 Wind profiles

The wind profiles at the wave measuring stations were measured for each reference wind speed, Ur, by using a standard Pitot-static tube and a Göttingen type manomtere. In almost every cases, the wind profiles near the air-water interface were found to follow a logarithmic distribution

$$U(z)=\frac{u_*}{\kappa}\ln\frac{z}{z_0}, \tag{1}$$

where $U(z)$ is the wind velocity at an elevation, z, over the mean water level, u_* is the friction velocity of the wind at the surface, κ is the von Kármán constant, and z_0 is the roughness parameter. As examples, the

Table-1 Wind data

U_rm/s	Station	F cm	u_* cm/s	$\bar{u}_*$ cm/s	z_0 cm	U_{10} m/s	γ^2_{10}
5.0	1	105	14.9	14.9	2.24×10^{-4}	5.7	6.85×10^{-4}
	2	225	22.2	18.5	2.40×10^{-3}	7.2	9.59×10^{-4}
	3	345	21.6	19.6	2.94×10^{-3}	6.9	9.91×10^{-4}
	5	585	21.6	20.1	3.05×10^{-3}	6.8	9.97×10^{-4}
	7	825	25.9	21.2	1.47×10^{-2}	7.2	1.29×10^{-3}
7.5	1	105	29.4	29.4	1.19×10^{-3}	10.0	8.63×10^{-4}
	2	225	34.3	31.8	4.79×10^{-3}	10.5	1.07×10^{-3}
	3	345	44.9	36.2	2.97×10^{-2}	11.7	1.48×10^{-3}
	5	585	49.6	39.5	4.28×10^{-2}	12.5	1.59×10^{-3}
	7	825	50.5	41.7	7.49×10^{-2}	12.0	1.77×10^{-3}
10.0	1	105	36.9	36.9	4.07×10^{-5}	12.9	8.16×10^{-4}
	2	225	51.2	44.0	1.06×10^{-2}	14.7	1.22×10^{-3}
	3	345	66.9	51.7	4.95×10^{-2}	16.6	1.63×10^{-3}
	5	585	64.5	54.9	3.99×10^{-2}	16.3	1.56×10^{-3}
	7	825	66.9	57.3	4.19×10^{-2}	16.8	1.58×10^{-3}
12.5	1	105	47.8	47.8	1.67×10^{-3}	15.9	9.05×10^{-4}
	2	225	64.2	56.0	1.53×10^{-2}	17.8	1.31×10^{-3}
	3	345	77.1	63.0	4.41×10^{-2}	19.3	1.59×10^{-3}
	5	585	80.9	67.5	5.33×10^{-2}	19.9	1.66×10^{-3}
	7	825	83.5	70.7	7.50×10^{-2}	19.8	1.78×10^{-3}
15.0	1	105	79.6	79.6	1.08×10^{-2}	22.7	1.23×10^{-3}
	2	225	109.0	94.3	8.76×15^{-2}	25.4	1.84×10^{-3}
	3	345	126.4	105.0	1.63×10^{-1}	27.5	2.11×10^{-3}
	5	585	157.2	118.0	3.83×10^{-1}	30.9	2.59×10^{-3}
	7	825	179.6	130.4	6.15×10^{-1}	33.2	2.93×10^{-3}

measured wind profiles at station No. 3 (F=345 cm) for five reference wind speeds, Ur=5, 7.5, 10, 12.5, and 15 m/sec, are shown in Fig. 9.

The friction velocity u_* and the roughness parameter z_0 were determined by fitting the logarithmic distribution (1) to the measured wind profiles. The measured values of u_* and z_0 are summarized in Table-1, where $\bar{u}_*$ is

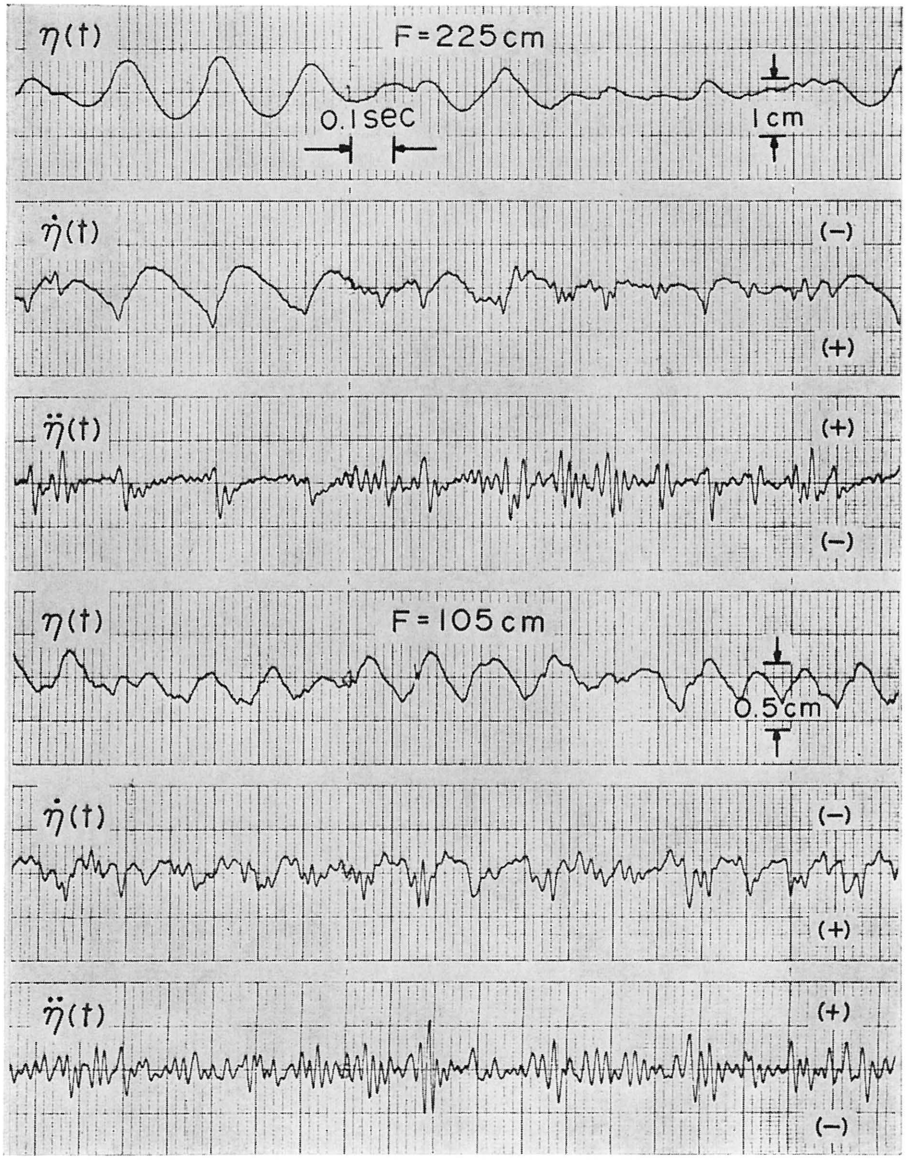

Fig. 10 Wave records η(t), $\dot{\eta}(t)$ and $\ddot{\eta}(t)$.
(F=105 cm, 225 cm, U_r=10 m/s)

the mean value of the local friction velocities which were measured at the stations within a fetch. For example, $\bar{u}_*$ at the station No. 3 is the mean value of the friction velocities measured at the stations No. 1, No. 2 and No. 3. In Table-1, U_{10} is the wind speed at $z=10$ m which is estimated from the logarithmic distribution of the wind, and γ_{10} is the drag coefficient of the water surface, *i.e*, $\gamma_{10}=u_*^2/U_{10}^2$.

3.2 The differentiated wave signals

Fig. 10 shows a part of the wave record monitored on the chart recorder, which contains records of the surface elevation η(t), its single differentiation, $\dot{\eta}(t)$, and its double differentiation, $\ddot{\eta}(t)$ at station No. 1 (F=105 cm)

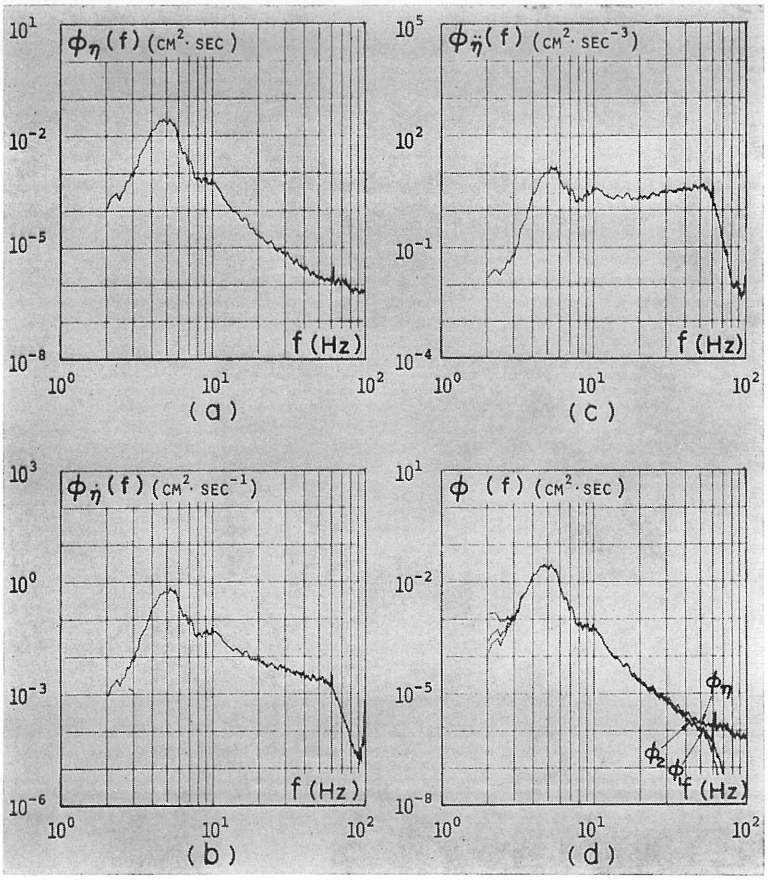

Fig. 11 (a) Frequency spectrum $\phi_\eta(f)$,
(b) Frequency spectrum $\phi_{\dot{\eta}}(f)$
(c) Frequency spectrum $\phi_{\ddot{\eta}}(f)$
(d) Relationships among $\phi_\eta(f)$, $\phi_{\dot{\eta}}(f)$ and $\phi_{\ddot{\eta}}(f)$
(F=345 cm, U_r=12.5 m/sec)

and those at station No. 2 (F=225 cm) respectively for a reference wind speed, Ur=10 m/s. It can be seen from Fig. 10 that the high frequency ripples superimposed on the dominant waves are greatly amplified in $\dot{\eta}(t)$ and even more in $\ddot{\eta}(t)$. Fig. 11 [(a), (b) and (c)] shows the surface elevation spectra, $\phi_\eta(f)$; the vertical surface velocity spectra, $\phi_{\dot{\eta}}(f)$ and the vertical surface acceleration spectra, $\phi_{\ddot{\eta}}(f)$. It shoud be mentioned that, in Fig. 11, the rapid decrease of the spectral densities of $\phi_{\dot{\eta}}(f)$ and $\phi_{\ddot{\eta}}(f)$ in the frequency rage $f>50$ Hz is due to the effect of the low-pass filters and not the sharp cut-off due to the viscous effects (COX[11]).

For ideal conditions, where the differentiations are performed perfectly and the spectral computations contain no errors, the following relationships are satisfied.

$$\phi_\eta(f)=\phi_{\dot{\eta}}(f)/(2\pi f)^2 \tag{2}$$

$$\phi_\eta(f)=\phi_{\ddot{\eta}}(f)/(2\pi f)^4 \tag{3}$$

In order to check equations (2) and (3), the measured spectra, $\phi_\eta(f)$, $\phi_{\dot{\eta}}(f)$ and $\phi_{\ddot{\eta}}(f)$ are compared in Fig. 11 (d) where $\phi_1=\phi_{\ddot{\eta}}(f)/(2\pi f)^2$ and $\phi_2=\phi_{\ddot{\eta}}(f)/(2\pi f)^4$. As can be seen from Fig. 10 (d), equations (2) and (3) are satisfied almost perfectly execept for slight differences in the high frequency range and in the low frequency range. Therefore, discussion of the high frequency wave spectra will be based only on the spectral data for $\phi_\eta(f)$ in this report.

3.3 Growth of the wave spectrum

Figs. 12a and 12b show the series of change of the one-dimensional wave spectrum at fetches of 345 cm and 825 cm when the wind speed was changed respectively for $Ur \doteqdot 5$ m/sec$\sim$15 m/sec. The following characteristics can be seen clearly from the figures; (1) the successive increase of the total spectral energy, (2) a shift of the frequency of the spectral maximum toward lower frequencies, and (3) a remarkable increase of the specral energy in some high frequency region.

In a previous study, MITSUYASU[3] proposed the following relations for the growth of the dominant part of the wave spectrum using the wind and wave data measured in a wave tank and in a bay:

$$\sqrt{\hat{E}}=1.31\times 10(\hat{F})^{0.504}, \tag{4}$$

$$\hat{f}_m=1.00(\hat{F})^{-0.330}, \tag{5}$$

where $\sqrt{\hat{E}}$ is the dimensionless wave energy

$$\sqrt{\hat{E}}=g\sqrt{E}/\bar{u}^2_*, \tag{6}$$

$$E=\int_0^\infty \phi(f)\ df \tag{7}$$

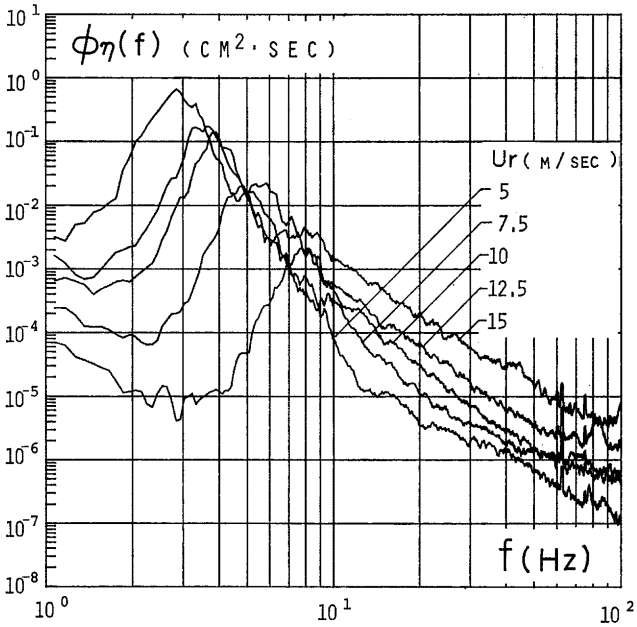

Fig. 12a Growth of the wave spectrum with wind speed. (F=345 cm, U_r=5, 7.5, 10, 12.5, 15 m/sec)

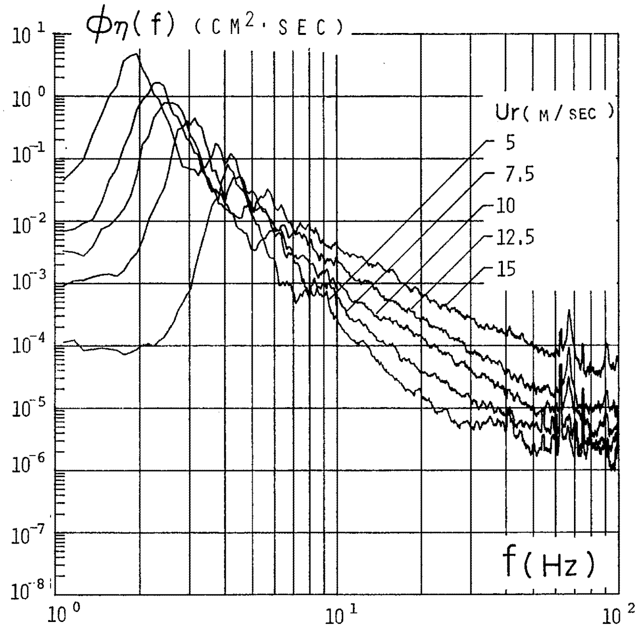

Fig. 12b Growth of the wave spectrum with wind speed. (F=825 cm, U_r=5, 7.5, 10, 12.5, 15 m/sec)

$\hat{F}$ is the dimensionless fetch

$$\hat{F}=gF/\bar{u}_*^2, \tag{8}$$

and $\hat{f}_m$ is the dimensionless frequency of the spectral maximum

$$\hat{f}_m=\bar{u}_*f_m/g, \tag{9}$$

In the above relations, $\bar{u}_*$, the mean value of the local friction velocities, is used instead of the local friction velocity u_*. This was done for the following reason. As previously shown in Table-1, the local friction velocity, u_*, changed with fetch, and the use of the local friction velocity in the fetch graph increased the scatter of the data.

Recently almost the same relations were obtained by the wave observations in the North Sea (HASSELMANN, et al [14]).

In order to verify the relations (4) and (5) by using the present data of laboratory wind waves, those dimensionless quantities and their interrelations were determined as shown in Fig. 13a and Fig. 13b. It can be seen from these figures that the present data on $\sqrt{\hat{E}}$, $\hat{f}_m$ and $\hat{F}$ satisfy quite well relations (4) and (5), though several points for $\sqrt{\hat{E}}$ are inconsistent with relation (4). The data for $\sqrt{\hat{E}}$ enclosed by the dot-dash line, which disagree with relation (4), correspond to the wave spectra measured at a

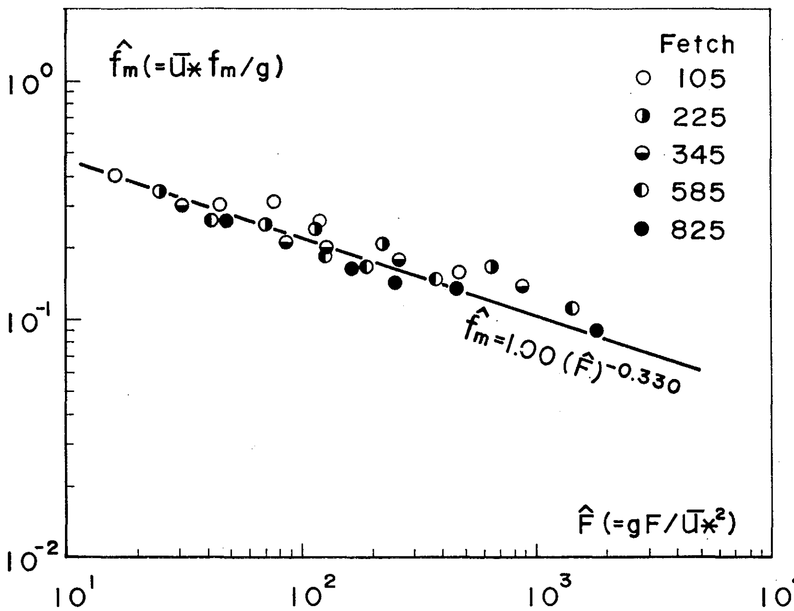

Fig. 13a Fetch relation (1): Dimensionless spectral peak frequency $\hat{f}_m$ versus dimensionless fetch $\hat{F}$.

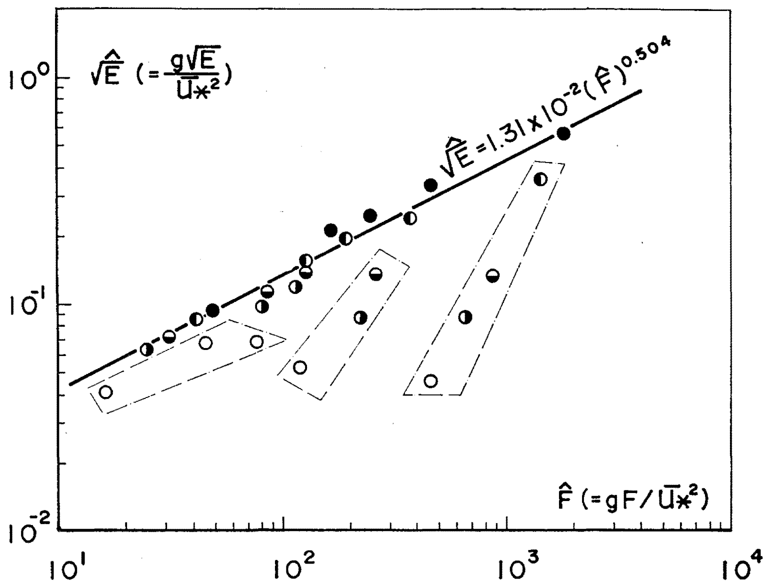

Fig. 13b Fetch realtion (2): Dimensionless wave height $\sqrt{\hat{E}}$ versus dimensionless fetch $\hat{F}$.

very short fetch (F=105 cm) and those measured for the low-speed wind (Ur=5 m/s). Such spectra may be considered to be a kind of undeveloped (unsaturated) spectra. Therefore, it can be said that fully developed spectra of fetch-limited wind waves follow quite well the relataions (4) and (5), but undeveloped spectra do not neccessarily follow relation (4). Relation (5) seems to be satisfied even in the undeveloped wave spectra.

The growth characteristics of the wave spectra at the high frequency region (f: 10~50 Hz) will be discussed separately in the next section. In Fig. 12, the complicated zigzag forms of the spectra at the very high frequency range ($f \gtrsim 60$ Hz), are considered to be due to electronic noise.

Since the low pass filters were not used in the measuring circuit for $\eta(t)$, as seen in Fig. 6, the noise which was mainly due to the power supply with a frequeney 60 Hz, might be induced in the electronic circuit.

4. Growth of the high frequency spectra of wind-generated waves.

As already shown in Fig. 12a and 12b, spectral density for high frequency region increases remarkably with increasing wind speed. The existence of such a strongly wind speed dependent region in the high frequency wave spectrum was discussed recently by PIERSON and STACY[10]. They proposed a wave number spectrum of fully developed ocean waves, $S(k)$, which consists of the following five regions;

1) the gravity wave-gravity equilibrium spectral range.

$$S_1(k)=4.05\times10^{-3}k^{-3}\exp\left[-0.74\,g^2/\{U_{19.5}(u_*)\}^4k^2\right],$$
$$\text{for } 0<k<k_1(=k_2u_{*m}{}^2/u_*{}^2). \tag{10}$$

2) the Kitaigorodskii spectral range

$$S_2(k)=4.05\times10^{-3}k_1{}^{-1/2}k^{-5/2},$$
$$\text{for } k_1<k<k_2(\cong0.359). \tag{11}$$

3) the Leykin-Rosenberg spectral range

$$S_3(k)=4.05\times10^{-3}D(u_*)k_3{}^{-p}k^{-3+p},$$
$$\text{for } k_2<k<k_3(\cong0.942). \tag{12}$$

4) the capillary spectral range

$$S_4(k)=4.05\times10^{-3}D(u_*)k^{-3},$$
$$\text{for } k_3<k<k_\nu. \tag{14}$$

5) the Cox viscous cut-off region

$$S_5(k)=1.473\times10^{-4}u_*{}^3k_m{}^6k^{-9},$$
$$\text{for } k_\nu<k<\infty. \tag{14}$$

where $U_{19.5}(u_*)$ is the wind speed at 19.5 m for the friction velocity u_*, $u_{*m}=12$ cm/sec. $k_m=(g/\gamma)^{1/2}=3.63(\gamma=\sigma/\rho_w$; σ is the surface tension and ρ_w is the density of water),

$$D(u_*)=(1.247+0.0268u_*+6.03\times10^{-5}u_*{}^2)^2, \tag{15}$$

$$p=\log_{10}\{D(u_*)/(u_*/u_{*m})\}/\log_{10}(k_3/k_2), \tag{16}$$

$$k_\nu=0.5756u_*{}^{1/2}\{D(u_*)\}^{-1/6}k_m. \tag{17}$$

The wave spectrum in the first range $S_1(k)$ is essentially the spectrum proposed by PIERSON and MOSKOWITZ, the high frequency part of which tends to the Phillips equilibrium form (PHILLIPS[15])

$$S_1(k)=4.05\times10^{-3}k^{-3} \tag{18}$$

The wave spectrum in the fourth range $S_4(k)$ is strongly wind speed dependent and the second and third ranges can be considered to be the spectral range that connect the first range and the fourth range. The fifth range was determined from slope spectra measured by COX[11].

In order to compare our measured spectra with those proposed by Pierson and Stacy measured frequency spectra $\phi(f)$ were transformed into the wave number spectra $S(k)$ by using the relations

$$S(k)\,dk=\phi(\omega(k))\cdot\frac{d\omega}{dk}dk \tag{19}$$

$$\phi(\omega)=(2\pi)^{-1}\phi(f), \tag{20}$$

and by assuming the dispersion relationship

$$\omega=\omega(k)=(gk+\gamma k^3)^{1/2}, \tag{21}$$

where $\omega(=2\pi f)$ is the angular frequency.

Fig. 14 (a) shows several examples of our measured wave number spectra normalized in the form

$$H(k, u_*)=S(k)k^3/4.05\times10^{-3}. \tag{22}$$

It can be seen from Fig. 14 (a) that there exists a wave number range ($k>1$) where the normalized spectra show roughly a constant value irrespective of the wave number k and that this constant value increases with increasing wind speed. Although these results are considered to support the spectral form (13) proposed by PIERSON and STACY for the capillary spectral range, closer examination of our present data shows that the normalized spectra are not actually constant with respect to wave number, k. They depend, in some cases, on k; that is, $H(k, u_*)$ decreases slightly with increasing k for the cases of low wind speed, $H(k, u_*)$ shows approximately a constant value for certain wind speeds, and beyond that wind speed $H(k, u_*)$ increases with k. The increasing rate is greater for higher wind speed. These characteristics

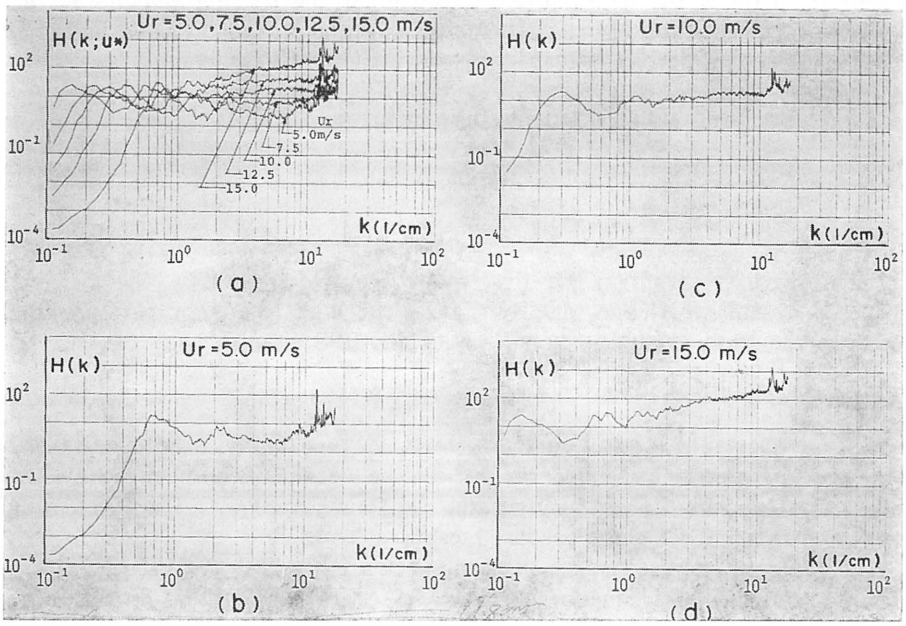

Fig. 14 Normalized wave spectra $H(k; u_*)$ and $H(k)$; (a) $F=825$ cm, $U_r=5$, 7.5, 10, 12.5, 15 m/sec, (b) $F=825$ cm, $U_r=5$ m/sec, (c) $F=825$ cm, $U_r=10$ m/sec, (d) $F=825$ cm, $U_r=15$ m/sec.

can be seen more clearly in Fig. 14 (b), (c) and (d) which show typical graphs of $H(k, u_*)$ selected from those shown in Fig. 14 (a).

These facts show that the spectral form (13) is not strictly satisfied for the capillary spectrum. In this connection, it should be noted that our measured spectra were frequency spectra instead of wave number spectra, and the latter were obtained from the former by using the dispersion relationship (21). If the dispersion relationship is slightly different from (21), say due to a drift current, $d\omega/dk$ changes and thus the form of $S(k)$ becomes slightly different from the present results. However, this problem will not be discussed further at this time, because we have no information on the properties of the drift current and its effects on the dispersion relationship.

In order to determine the new form of $D(u_*)$ in (13) from the present data by neglecting tentatively the trend in $H(k, u_*)$, mentioned adove, the quantity $D(u_*)$ was computed as

$$D(u_*)=\frac{1}{k_c-3k'_m}\int_{3k'_m}^{k_c} H(k, u_*)\ dk, \tag{23}$$

where $3k_m'$ is a wave number corresponding to the frequency, $3f_m$, and k_c is the wave number corresponding to the cut-off frequency f_c which was taken tentatively as 50 Hz for the data at stations No. 1, No. 2, and No. 3 and as 40 Hz for the data at stations No. 5 and No. 7. These cut-off frequencies were selected as the upper limits of the frequency ranges where the amplitude response factors of the wave gauges are almost unity and also the effects of noise are negligible. The wave number $3k_m'$ was selected as the lower limit of integration, because the non-linear effects of the frequency components near the frequency of the spectral maximum f_m produced a secondary and tertiary peaks of the spectrum near frequencies, $2f_m$ and $3f_m$, and they introduced some difficulties for the accurate determination of $D(u_*)$. Therefore, the frequency range $3f_m<f<f_c$ was selected so that the spectral density in that range could not be affected by such nonlinear effects. Accrding to PIERSON and STACY the capillary spectral range was defined as

$$k_3(=0.92)<k<k_\nu. \tag{24}$$

Within a range of our presnt data, $3k_m'$ was always greater than $k_3(=0.92)$. The value of k_ν estimated from (17) was greater than k_c for every cases $U_r>10$ m/s, but it was a little smaller than k_c for some cases $U_r<7.5$ m/s. However, sharp fall of the spectrum was not found even in the latter cases. Therefore, the wave number range (23) is considered to be well included in the capillary spectral range defined by PIERSON and STACY.

Fig. 15 shows a plot of $D(u_*)$ versus u_* on a logarithmic scale, where the functional form of $D(u_*)$ proposed by PIERSON and STACY is shown by a full line. The experimental data surrounded by the dot-dash-line correspond to the spectra for which "k^{-3} law" is not strictly satisfied. It can

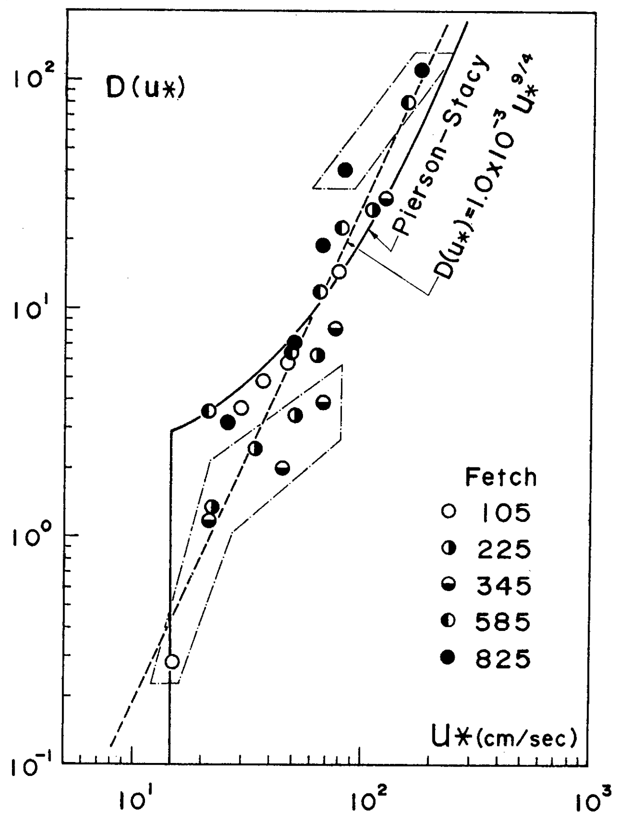

Fig. 15 $D(u_*)$ versus u_* for the capillary spectral range.

be seen from Fig. 15 that the functional form for $D(u_*)$ proposed by PIERSON and STACY is fairly consistent with our present data except for several points that do not follow the "k^{-3} law". However, if all of the present data are used for determining the functional form of $D(u_*)$ its form can be given approximately by

$$D(u_*)=1.0\times10^{-3}u_*^{9/4}. \tag{25}$$

Fig. 15 also shows that there are no definite relations between $D(u_*)$ and fetch F, though it is difficult to conclude that $D(u_*)$ is independent of F.

Recently, TOBA proposed the following spectral form for the high frequency side of the one-dimensional spectrum in the gravity wave range:

$$\phi(f;u_*)=\alpha_g(2\pi)^{-3}gu_*f^{-4}, \tag{26}$$

where $\alpha_g(=0.02)$ is a universal costant.

Furthermore, as an extended form of the spectrum (26), in which the capillary range is included, he proposed the spectral form

$$\phi(f, u_*) = \alpha_g (2\pi)^{-3} g_* u_* f^{-4}, \tag{27}$$

where

$$g^* = g + \gamma k^2. \tag{28}$$

To compare our experimental data with the spectral form (27), measured spectra $\phi(f)$ were normalized in the form

$$G(f, u_*) = \phi(f) \cdot (2\pi)^3 f^4 / g_* u_*. \tag{29}$$

Fig. 16 (a) shows several examples of the normalized spectra $G(f; u_*)$ which were measured at the station No. 7 (F=825 cm) for the wind speeds

U_r: 5, 7.5, 10, 12.5, 15 m/s

Typical spectra are picked from Fig. 16 (a) and are shown separately in Fig. 16 (b), (c) and (d). It can be seen from these figures that in some high friquency region $3f_m < f < 60$ Hz, the normalized spectrum $G(f; u_*)$ shows roughly constant values irrespective of the frequency f, though there exists "the overshooting effects", i.e., the excess energy accumulation near the frequencies f_m, $2f_m$ and $3f_m$. The complex zigzag form of $G(f; u_*)$ in

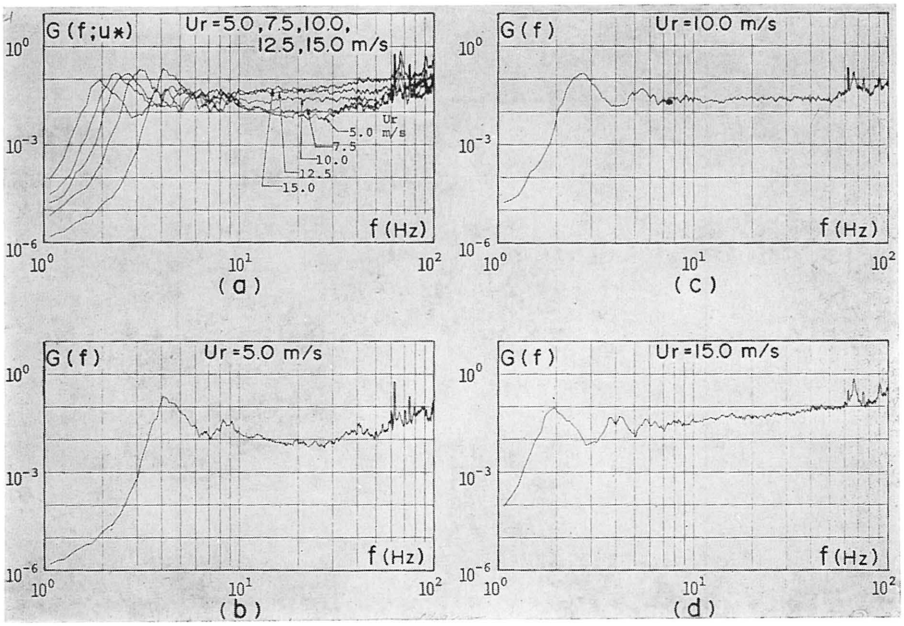

Fig. 16 Normalized wave spectra $G(f; u_*)$ and $G(f)$; (a) F=825 cm, U_r=5, 7.5, 10, 12.5, 15 m/sec, (b) F=825 cm, U_r=5 m/sec, (c) F=825 cm, U_r=10 m/sec, (d) F=825 cm, U_r=15 m/sec.

a frequency range $f>60$ Hz is considered to be due to the effct of noise.

According to TOBA, $G(f;u_*)$ approaches to a universal constant α_g (=0.02) in the high frequency region of the spectrum. However, present results show that α_g in the expression (27) is not a universal constant but it depends, to a certain extent, on the friction velocity u_*. To examine such characteristics more quantitatively α_g was determined from the measured spectra as

$$\alpha_g=\frac{1}{f_c-3f_m}\int_{3f_m}^{f_c}G(f;u_*)\,df. \tag{30}$$

where the range of the integration, $3f_m\sim f_c$, corresponds to that in (23).

Fig. 17 shows a plot of α_g versus u_* on a logarithmic scale. It can be seen from Fig. 17 that α_g increases with the friction velocity u_*. Closer examination of the figure reveals that the increasing rate of α_g with u_* is fairly small for $u_*<50$ cm/s, and it increases rapidly for $u_*>50$ cm/s, and that α_g depends, to a certain extent, on the fetch F, though an exact relationship between α_g and F is not clear at this time.

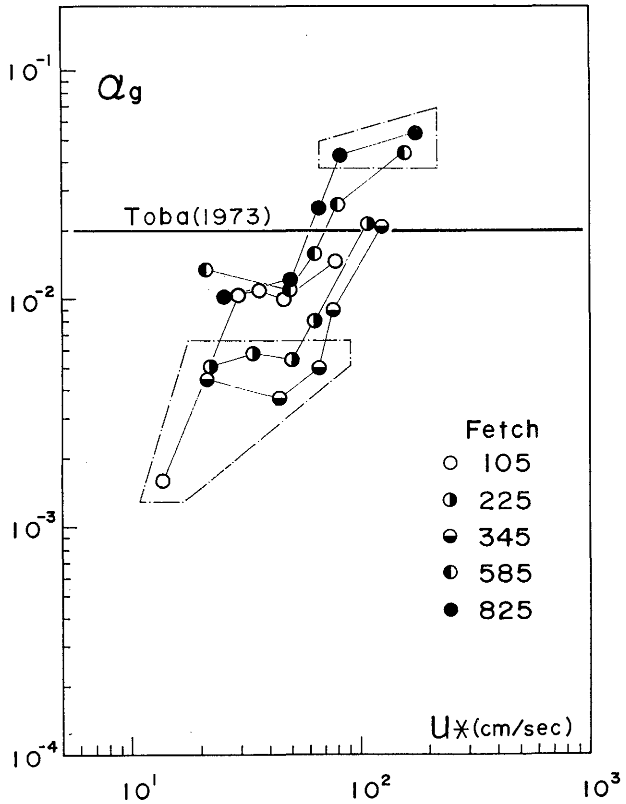

Fig. 17 α_g versus u_* for the capillary spectral range.

It should be noted here that, as can be seen from Fig. 16, $G(f;u_*)$ is not strictly constant even in the frequency range $3f_m<f<f_c$, but it shows a trend that is similar to that shown in $H(k, u_*)$. That is, $G(f; u_*)$ decreases slightly with increasing f for the cases of low speed wind, $G(f;u_*)$ shows constant values for certain wind speeds, and beyond that wind speed, $G(f;u_*)$ increases with f. The experimental data in Fig. 17 enclosed by the dot-dash-line correspond to such spectra that show the trend in $G(f; u_*)$ mentioned above. However, comparing Fig. 14 and Fig. 16, we can say that the dependence of $G(f;u_*)$ on f is smaller than that of $H(k; u_*)$ on k.

5. Discussion

It should be worthwhile to add some comments on the definition of the capillary range of the wave spectrum. In a strict sense, it is fairly difficult to define the different spectral ranges, because the effects of the different controlling factors change continously with the frequency or wave number, and clearly there are no definite boundaries of the spectral ranges.

Concerning the capillary specrtal range proposed by PIERSON and STACY, the wave number

$$k_3=0.942, \quad (f\cong 5.0\text{Hz}), \tag{31}$$

which is defined as the lower boundary of the capillary spectral range, corresponds to the wave number at which the effect of the surface tension attains approximately to 10% of that of gravitational acceleration. In some cases the wave number,

$$k_{gs}=(g/\gamma)^{1/2}=3.64, \quad (f_{gs}\cong 13.4\text{ Hz}), \tag{32}$$

at which the effect of surface tension is equal to that of gravitational acceleration, is used as an index for the capillary waves (PHILLIPS [16]).

If we define k_s as the wave number at which the effect of the surface tension is ten times as large as that of gravitational acceleration, it is

$$k_s=(10g/\gamma)^{1/2}=11.5, \quad (f_s=56\text{ Hz}). \tag{33}$$

In this case k_s can be considered as the wave number beyond which the wave spectrum is conrolled mainly by the effect of the surface tension of the water. Consequently, the spectral range,

$$\begin{aligned} &k_3(=0.942)<k<k_s(=11.5),\\ &f_3(\cong 5.0\text{Hz})<f<f_s(\cong 56\text{ Hz}), \end{aligned} \tag{34}$$

can be considered as the gravity-capillary spectral range where both the gravitational acceleration and the surface tension are the controlling factors for the wave spectrum, though the weight of each factor changes with k or f. The high frequecy parts of our measured spectra are included approximately in the spectral range (34).

The spectral range, $k>k_s$, correponds to the pure capillary range. Assuming

$$g\ll\gamma k^2, \tag{35}$$

the forms of the pure capillary spctrum can be derived respectively from the PIERSON and STACY spectrum (13) and from the TOBA spectrum (27). That is, from (13), (19) and (21) the PIERSON and STACY spectrum for the pure capillary range is given by

$$S(\omega)=2.7\times10^{-3}D(u_*)\gamma^{2/3}\omega^{-7/3}, \tag{36}$$

and from (20), (27) and (28) the TOBA spectrum in that range is given by

$$\phi(\omega)=\alpha_g u_*\gamma^{1/3}\omega^{-8/3}. \tag{37}$$

Equation (36) is similar to the spctral form proposed by PHILLIPS[16] on dimensional grounds, the PHILLIPS form of the pure capillary spectrum having been suggested originally by HICKS (see PHILLIPS[16]). However, it may be difficult to measure the pure capillary spectra in the form (36) or (37). Because the effect of viscosity of the water becomes increasingly important for the waves in the pure capillary range, and it will change the spectral form (36) or (38) into the other form like "COX viscous cut-off region" determined by PIERSON and STACY.

We have so for neglected the discussion on the PHILLIPS equilibrium form of the wave spectrum in the gravity range. As shown in Fig. 16 the high frequency side of each spectrum is greatly affected by nonlinear effects due to the spectral components near the dominant peak of the wave spectrum. Such characteristics of the wave spectrum in the high frequency side of the spectral peak have been named "overshoot" and "undershoot". This effect can be frequently observed in the laboratory wave spectra. In our previous study, for example, the equilibrium constant β have been determined by taking a kind of smoothing of the spectral densities (MITSUYASU[17]). In order to check the PHILLIPS equilibrium form very accurately by using the spectral data of wind waves generated in the laboratory tank, the wind-wave tank should be long enough to generate the wind waves with a peak in a low frequency range.

Let us consider next the equilibrium form of the capillary wave spectrum. According to the results shown in Fig. (15) or Fig. (17), it is difficult to recognize the existence of the equilibrium spectrum in the gravity-capillary range at least for the winds up to $u_*=180$ cm/s ($U_{10}=33$ m/s). Even for the higher wind speed, it is difficult to expect the existence of the saturated spectrum in the high frequency range of the wave spectrum as shown in the following discussion. According to the visual observation of the wind waves generated in our present experiment, the dominant waves and superimosed capillary waves begin clearly to break near at the friction velocity $u_*=50$ cm/

sec ($U_r=10$ m/sec), and the water surface becomes successively more irregular (c.f. Fig. 18). With increasing wind speed, the breaking of the waves becomes more and more violent, and air bubbles are carried below the water surface by the breaking of the waves of various scales and by the possible action of vorticity in the highly turbulent drift current. For the cases of very high wind speed, water particles are carried into the air above the water surface simultaneously with the entrainment of the air bubbles into the water, and the mixing processes of the air and water develop. For such situations it is difficult not only to define the water surface but also to give a physical meaning for the measured high frequency spectrum of the irregular water surface where the air and the water are mixed.

Finally, the quantity $D(u_*)$ in the PIERSON and STACY spectrum will be discussed. On dimensional grounds, $D(u_*)$ in (12) or (13) must be a dimensionless quantity. A simple way to satisfy this condition is to replace u_* in $D(u_*)$ by a dimensionless velocity.

A reasonable assumption for the dimensionless velocity $\hat{u}_*$ is

$$\hat{u}_*=\left(\frac{\rho_a}{\rho_w}\right)^{1/2}\frac{k^{1/2}}{g_*^{1/2}}u_*, \tag{38}$$

which represents the ratio of the wind action on the water surface to the restoring force for the water surface. If further $D(u_*)$ is assumed simply as

$$D(\hat{u}_*)=A\hat{u}_*=A\left(\frac{\rho_a}{\rho_w}\right)^{1/2}g_*^{-1/2}u_*k^{1/2}, \tag{39}$$

where A is a dimensionless constant, (13) reduces to

$$S_4(k)=5.05\times10^{-3}A\left(\frac{\rho_a}{\rho_w}\right)^{1/2}g_*^{-1/2}u_*k^{-5/2}. \tag{40}$$

Denoting

$$5.05\times10^{-3}A\left(\frac{\rho_a}{\rho_w}\right)^{1/2}=\frac{1}{2}\alpha_g, \tag{41}$$

(40) reduces to the following wave number spectrum proposed by TOBA*

$$\phi_{kg}=\frac{1}{2}\alpha_g g_*^{-1/2}u_*k^{-5/2}. \tag{42}$$

However, as previously shown, α_g is not a universal dimensionless constant but depends on u_*. This fact means that the assumption (39) for the form of $D(u_*)$ is not an appropriate one. The determination of a resonable dimensionless form for $D(u_*)$ is one of the subjects for future study.

---

*The wave number spectrum (42) obtained by TOBA is not consistent with his frequency spectrum (27), because the conversion relation (19) is not satisfied between (27) and (42). The corrected wave number spectrum is given by

$$\phi_{kg}=\frac{1}{2}\alpha_g g_*^{-1/2}(1+2\gamma k^2/g_*)u_*k^{-5/2}.$$

Acknowledgements

We would like to express our sincerest appreciation to Dr. W. J. PIERSON for valuable discussions during this study and for penetrating comments on the first draft of this paper. We are deeply indebted to Dr. Y. TOBA of Tohhoku University and Dr. S. MIZUNO for their valuable comments on the first draft of this paper. We are also indebted to Mr. K. ETO and Miss S. NOGUCHI for their assistance in the course of the present study.

References

1) Neumann, G.: On ocean wave spectra and a new method of forcasting wind-generated sea. Beach Erosion Board, U. S. Army Corps of Engineers, Tech. Memo. No. 43, 1953, 42pp.
2) Pierson, W. J. and Moskowitz, L.: A proposed spectral form for fully developed wind seas based on the similarity theory of S. A. Kitaigorodskii. J. Geophys. Res. 69, 1964, 5181-5190.
3) Bretschneider, C. L.: A one-dimensional gravity wave spectrum, Ocean Wave Spectra, Englewood Cliffs, N. J., Prentice Hall Inc. 1963, pp. 41-56.
4) Mitsuyasu, H.: The one-dimensional wave spectra at limited fetch, Proc. 13 th Coastal Eng. Conf., Vancouver, Vol. 1, 1972, pp. 289-306.
5) Munk, W. H.: Wind stress on water; an hypothesis, Q. J. Roy. Met. Soc., 81, 1955, pp. 320-332.
6) Longuet-Higgins, M. S.: A nonlinear mechanism for the generation of sea waves, Proc. Roy. Soc. A. 311, 1969, pp. 371-389.
7) McGoldrick, L. F.: Resonant interactions among capillary-gravity waves, J. Fluid Mech. 21, 1965, pp. 305-332.
8) Valenzuela, G. R. and Laing, M. B.: Nonlinear energy transfer in gravity-capillary wave spectra, with applications. J. Fluid Mech. 54, 1972, pp. 507-520.
9) Pierson, W. J., Jackson, F. C., Stacy, R. A. and Mehr, E.: Research on the problem of the radar return from a wind roughened sea. Advanced Applications Flight Experiments Principal Investigators Review, Oct. 5-6, NASA Langley Research Center, 1971, pp. 83-114.
10) Pierson, W. J. and STACY, R. A.: The elevation, slope, and curvature spectra of wind roughened sea surface. NASA Contractor report CR 2247, 1973, pp. 128.
11) Cox, C. S.: Measurements of slopes of high frequency wind waves. J. Mar. Res. 16, 1958, pp. 199-225.
12) Toba, Y.: Local balance in the air-sea boundary process 111. J. Oceanog. Soc. Japan, 29, 1973, pp. 209-220.
13) Mitsuyasu, H.: On the growth of the spectrum of wind-generated waves 1. Rep. Res. Inst. Appl. Mech., Kyushu Univ., Vol. 16, No. 55, 1968, pp. 459-482.
14) Hasselmann, K., et al.: Measurements of wind-wave growth and swell decay during the Joint North Sea Wave Project (JONSWAP), Dtsch. Hydrogr. Z. 12, 1973, pp. 1-95.
15) Phillips, O. M.: The equilibrium range in the spectrum of wind-generated waves, J. Fluid Mech. 4, 1958, pp. 426-434.
16) Phillips, O. M.: ***The dynamics of the upper ocean***, Cambridge University Press. 1966, pp. 118.
17) Mitsuyasu, H.: On the growth of the spectrum of wind-generated waves 11. Rep. Res. Inst. Appl. Mech., Kyushu Univ., Vol. 17, No. 59, 1969, pp. 235-248.

(Recieved November 30, 1974)

Fig. 18 Photographs of waves in a wind-wave channel for a fetch $F=825$ cm. Wind speeds are, from the top to the bottom, U_r: 5, 7.5, 10, 12.5, 15 (m/sec).

U_r(m/sec)

5

7.5

10

12.5

15

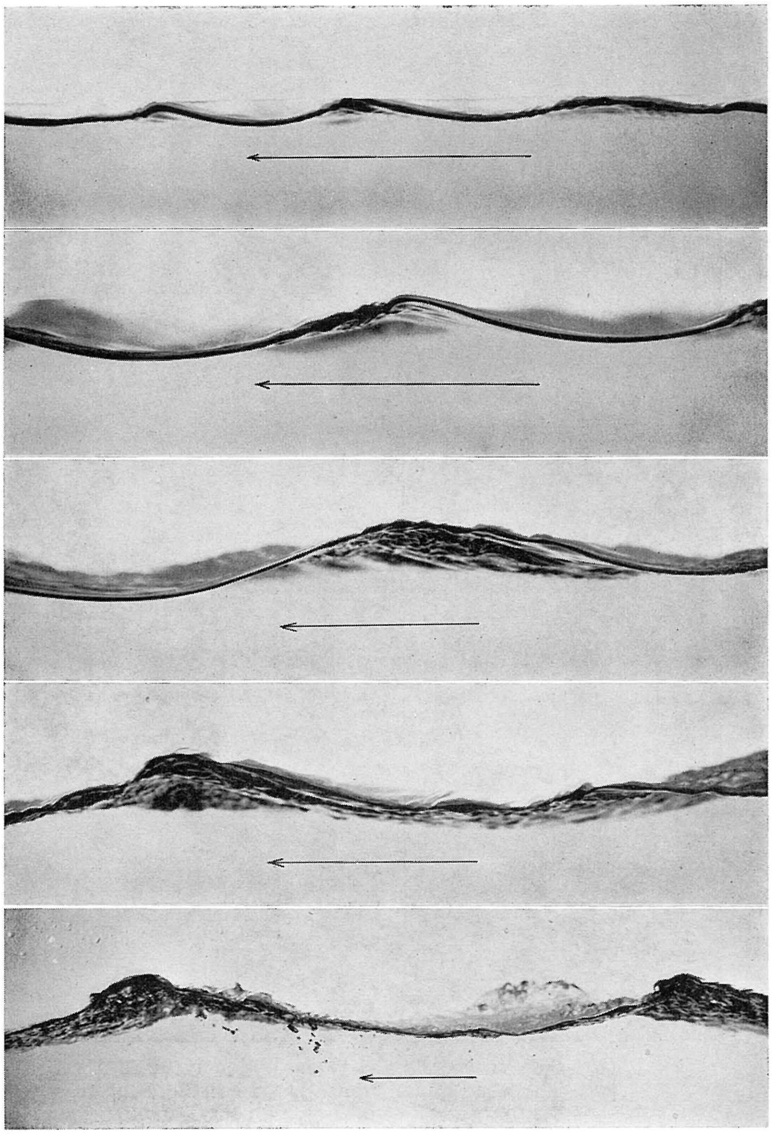

(a) Side view of waves
Arrow is 10 cm in length and shows the direction of wave propagation.

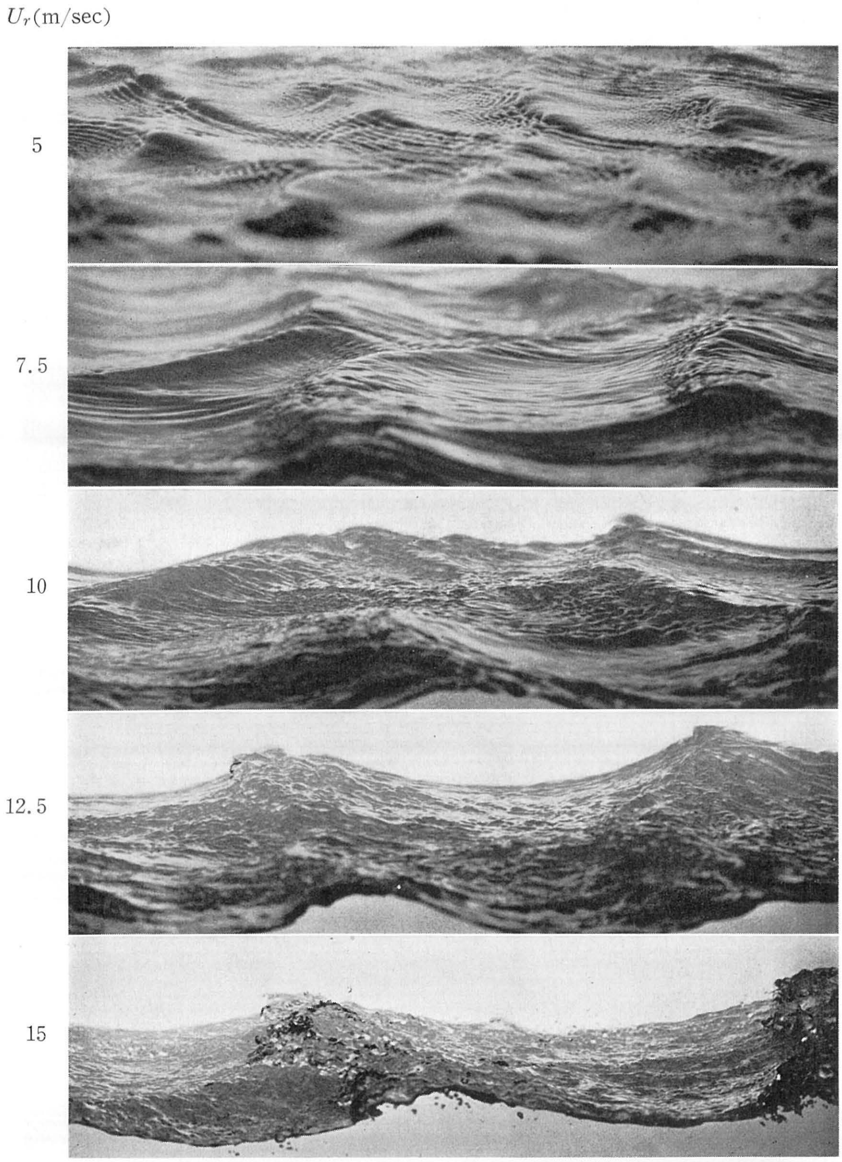

(b) Side view of waves (from obliquely upside).
The scale of the figure is almost the same to that for Fig. 18(a).

U_r(m/sec)

5

7.5

10

12.5

15

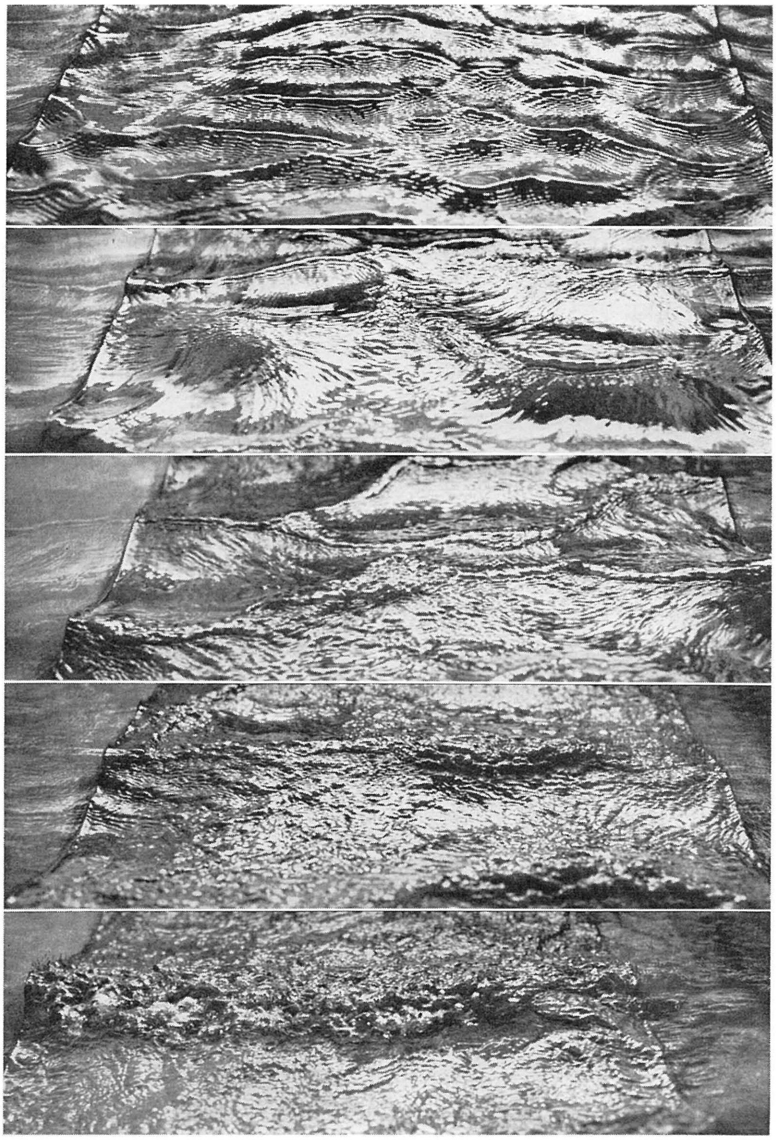

(c) Bird's-eye view of waves (from obliquely down wind side). Wave direction is from upside to downside.